Electronic Supplementary Material (ESI) for Energy & Environmental Science.

Electronic Supplementary Information

Atomically Dispersed Fe-N-C Decorated with Pt-alloy Core-shell Nanoparticles for Improved Activity and Durability towards Oxygen Reduction

Xiang Ao,[ab] Wei Zhang,[c] Bote Zhao,*[a] Yong Ding,[a] Gyutae Nam,[a] Luke Soule,[a] Ali Abdelhafiz,[a] Chundong Wang*[b] and Meilin Liu*[a]

[a] School of Materials Science and Engineering, Georgia Institute of Technology, Atlanta, Georgia 30332, United States. E-mail: bote.zhao@mse.gatech.edu, meilin.liu@mse.gatech.edu
[b] Wuhan National Laboratory for Optoelectronics, School of Optical and Electronic Information, Huazhong University of Science and Technology, Wuhan 430074, China. E-mail: apcdwang@hust.edu.cn
[c] Beijing Advanced Innovation Center for Soft Matter Science and Engineering, Beijing University of Chemical Technology, Beijing 100029, China

Table of Contents

1. Experimental and Computational Section

2. Supplementary Figures S1-S23

3. Supplementary Tables S1-S6

4. References

1. Experimental and Computational Section

Chemicals

Zinc nitrate hexahydrate ($Zn(NO_3)_2 \cdot 6H_2O$), 2-methylimidazole, ferric chloride ($FeCl_3 \cdot 6H_2O$), chloroplatinic acid hexahydrate ($H_2PtCl_6 \cdot 6H_2O$), methanol, ethanol, ethylene glycol, hexane and perchloric acid ($HClO_4$) were purchased from Sigma Aldrich. Commercial Pt/C (20 wt.%, HiSPEC3000) was purchased from Alfa Aesar and Nafion dispersion (5 wt.%) was obtained by diluting a Nafion D2021 dispersion. All the chemicals were used without any further purification procedure. The ultrapure water (18.2 MΩ·cm) used in all experiments was obtained through ion-exchange and filtration.

Preparation of ZIF-8

In a typical synthesis, $Zn(NO)_3 \cdot 6H_2O$ (1.762 g) was dissolved in 120 mL of methanol with stirring, then 2-methylimidazole (3.912 g) in 120 mL of methanol was poured into above solution followed by vigorous stirring for 6 h at room temperature. The as-obtained product was centrifuged and washed with methanol several times and finally dried overnight in oven at 80 ^oC.

Preparation of Fe_{SA}-N-C

Typically, ZIF-8 (100 mg) was dispersed in 16 mL of hexane by sonication for 1 h at room temperature. Then, 60 μL of $FeCl_3 \cdot 6H_2O$ aqueous solution (20 mg mL^{-1}) was added dropwise to the above solution under ultrasound for 10 min to get a homogeneous suspension. The suspension was stirred for another 2 h at room temperature. The impregnated ZIF-8 sample was then centrifuged and dried in oven at 60 ^oC overnight. Finally, the dried powders of impregnated ZIF-8 were placed in a tube furnace and annealed at 900 ^oC for 2 h with a heating rate of 5 ^oC min^{-1} under flowing Ar gas and then naturally cooled to room temperature to obtain Fe_{SA}-N-C.

Preparation of Pt_A@Fe_{SA}-N-C

At first, the Pt nanoparticles were deposited on Fe_{SA}-N-C via a surfactant-free reduction process in alkaline ethylene glycol.[1] Typically, 8 mg Fe_{SA}-N-C was dispersed in 4 mL of ethylene glycol containing 62 mM NaOH by sonication. Then, 4 mL of ethylene glycol containing 2.5 mM $H_2PtCl_6 \cdot 6H_2O$ was added into the above slurry under ultrasound followed by stirring for 30 min. The mixture was heated for 90 min with stirring at 160 ^oC in an oil bath. After cool down, the as-obtained Pt@Fe_{SA}-N-C were collected by centrifugation and washed with distilled water several times and finally dried in vacuum at 60 ^oC overnight. To transform Pt nanoparticles into structurally ordered Pt_3M intermetallic nanoparticles, the Pt@Fe_{SA}-N-C was further annealed at 900 ^oC for 30 min with a heating rate of 10 ^oC min^{-1} under flowing Ar gas and then naturally cooled to room temperature to obtain Pt_A@Fe_{SA}-N-C.

Preparation of N-C

ZIF-8 (100 mg) was placed in a tube furnace and annealed at 900 ^oC for 2 h with a heating rate of 5 ^oC min^{-1} under flowing Ar gas and then naturally cooled to room temperature, with the as-obtained sample denoted as N-C.

Preparation of Pt_A@N-C

The synthesis procedure of Pt_A@N-C was similar to that of the abovementioned Pt_A@Fe_{SA}-N-C, except for using N-C as a substrate for Pt deposition instead of Fe_{SA}-N-C.

Physical characterization

Scanning electron microscopy (SEM) analysis was performed on a Zeiss Ultra 60 FE-SEM with a beam voltage of 8 kV. An aberration-corrected scanning transmission electron microscope (STEM, Hitachi HD 2700) was used to analyze the detailed morphology and structure information. Powder X-ray diffraction (XRD) patterns of samples were recorded using an X'Pert PRO Alpha-1 X-ray diffractometer with a Cu Kα radiation source. Raman spectroscopic measurement was performed using a Renishaw RM1000 microspectroscopic system with an Ar laser excitation (514 nm). X-ray photoelectron spectroscopy (XPS) measurements were recorded with a Physical Electronics PHI 5802, and all the reported binding energy data were calibrated using C 1s (284.6 eV). The nitrogen adsorption–desorption isotherm of the sample was measured using a Micromeritics ASAP 2020 analyzer. The X-ray absorption fine structure (XAFS) analysis was performed on the BL10C beamline at the Pohang light source (PLS) with top-up mode operation under a ring current of 300 mA at 3.0 GeV. The acquired data were normalized to the incoming incident photon flux and processed according to the standard procedure using the ATHENA module implemented in the IFEFFIT software packages. To obtain quantitative structural parameters around central atoms, least-squares curve parameter fitting was performed using the ARTEMIS module of IFEFFIT software packages. The Pt content was confirmed by inductively coupled plasma optical emission spectrometer (ICP-OES, Varian 710ES).

Electrochemical measurements

Electrochemical measurements were carried out using an electrochemical workstation (Solartron SI 1287) with a standard three-electrode cell and a rotating disk electrode (RDE) system (Pine Instrument Company, USA). The RDE with a glassy carbon disk of 5 mm in diameter was used as the substrate for the working electrode. To prepare the working electrode, 2 mg of catalyst was ultrasonically dispersed in a 1.0 mL mixture of isopropanol (200 uL), water (796 uL) and Nafion (5 wt.%, 4 uL) solution to form an ink. Then 10 uL of the ink was drop-casted on the disk electrode and dried at room temperature using a rotational drying method to obtain a film electrode with a catalyst mass loading of 0.1 mg cm^{-2}. The rotational drying method was described in the previous work.[2] Typically, the aliquot of the well-dispersed ink was pipetted on the glassy carbon electrode substrate mounted on the inverted rotator and then the electrode was rotated at 700 r.p.m. until the film was dry. A Ag/AgCl electrode (4 M KCl solution) and a graphite rod were used as reference and counter electrode, respectively. All of the potentials reported in this work were calibrated to the reversible hydrogen electrode. A 0.1 M $HClO_4$ aqueous solution was used as electrolyte. The electrolyte was purged with required gas for at least 30 min before the test and the gas flow was maintained during the test. Cyclic voltammetry (CV) test was carried out in a N_2-saturated 0.1 M $HClO_4$ aqueous solution at a scan rate of 200 mV s^{-1}. The ORR activity was evaluated by linear sweep voltammetry (LSV) in O_2-saturated electrolyte collected by scanning anodically for Pt-containing catalysts and cathodically for non-Pt catalysts at a scan rate of 10 mV s^{-1}, and all currents were corrected by deducting the background current that measured in N_2-saturated electrolyte, and all potentials were corrected with ohmic loss.

PEMFC electrochemical performance test

The PEMFC electrochemical performance was tested at a fuel cell test system (a Scribner Associates Model 890 CL load box equipped with a Teledyne Medusa test station). The MEAs with an active area of 4 cm^2 were prepared using the spray deposition method.[3,4] Nafion 211 proton exchange membranes were purchased from Fuel Cell Store and treated with 5 wt. % H_2O_2 and 0.5 M H_2SO_4 solutions in the water bath at 80 ^oC for 1 h for each step, and then washed with deionized water before use. The catalyst ink was prepared by ultrasonically mixing the catalyst powder (2 mg), isopropanol (2 mL) and 5 wt. % Nafion ionomer solution (22 mg) for 1 h. Then the ink was sprayed on the one side of a pretreated Nafion 211 membrane at a hot plate (130 ^oC) to form the cathode catalyst layer. A commercial Pt/C catalyst (HiSPEC 3000) was deposited at the anode side by the similar method. The Pt loading was 0.2 mg cm^{-2} at the anode and 0.13 mg cm^{-2} at the cathode, respectively. The GDL (Sigracet 39 BC) was purchased from Fuel Cell Stores and used without further treatment. For H_2-O_2 fuel cell test, humidified hydrogen (150 mL min^{-1}) and oxygen (300 mL min^{-1}) were fed to the anode and cathode, respectively. The temperature of the cell was maintained at 65 ^oC and the backpressure of both the anode and cathode was 1 bar.

Computational section

All the calculations were performed by using the Vienna ab initio Simulation Package (VASP 5.4) code.[5-7] The generalized gradient approximation (GGA)[8] in the formalism of Perdew-Burke-Ernzerhof (PBE)[9] was adopted to describe the electronic exchange-correlation energy. The projector augmented wave (PAW) pseudo-potentials[10] were chosen to describe ionic cores. To improve the description of the adsorption of O, OH, and OOH on the catalysts, we employed the van der waals (VDW) correction proposed by Grimme, namely, the D3 framework.[11] A cutoff energy of 500 eV was selected through several testing calculations. The convergence threshold for the iteration in self-consistent-field (SCF) calculation was set at 10^{-5} eV, and that for geometry optimizations by using BFGS algorithm was set at 0.01 eV/Å on the maximum force component. The k-point sampling of the Brillouin zone was generated automatically by using the Monkhorst-Pack k-point mesh with a $3\times3\times1$ grid for the structure relaxation. A vacuum slab exceeding 15 Å was employed in z direction so that interaction between two neighboring surfaces can be neglected. The PBE exchange-correlation functional has the tendency to delocalize unpaired electrons and thus may not give accurate account of magnetic moment of Fe atom. To address this delocalization issue, the PBE+U method is employed[12] so that the localized 3*d* electron correlation for Fe atom can be corrected via the on-site coulomb and exchange interactions. Following the rotationally invariant approach used in previous studies,[12-14] the corresponding U values for Fe atoms is taken to be 3.29 eV.

The adsorption energies of ORR/OER intermediates on Pt (100), Fe-N_4 and Pt (100)/Fe-N_4 electrocatalyst systems were calculated based on the reversible hydrogen electrode (RHE) model proposed by Nørskov *et al*,[15] relative to $H_2O(g)$ and $H_2(g)$:

$$\Delta E_{O^*} = E_{O^*} + E_{H_2} - E_{H_2O} - E_* \quad (1)$$

$$\Delta E_{OH^*} = E_{OH^*} + 1/2E_{H_2} - E_{H_2O} - E_* \quad (2)$$

$$\Delta E_{OOH^*} = E_{OOH^*} + 3/2E_{H_2} - 2E_{H_2O} - E_* \quad (3)$$

where, E_*, E_{O^*}, E_{OH^*}, and E_{OOH^*} are the total energies of catalyst without and with the adsorption of O, OH and OOH, respectively. E_{H_2} and E_{H_2O} are the total energies of free H_2 and H_2O molecules in gas phases, respectively. The adsorption free energies can be obtained by the following equation:

$$\Delta G = \Delta E + \Delta ZPE - T\Delta S + \Delta G_U + \Delta G_{pH} \quad (4)$$

where, ΔZPE and ΔS are the change in zero point energies (ZPE) and entropy (S) during the reaction. ΔG_U is electrons transfer in the electrode, and ΔG_{pH} is the effect of pH value of the electrolyte. We describe in more detail how to get these values including the ΔZPE, ΔS, ΔG_U, and ΔG_{pH} in the supporting information. It is known that OH and OOH can form hydrogen-bond with H_2O due to the solvent effect,[16,17-19] which can lower the adsorption free energies of OH^* and OOH^*. So, in this work, the 0.3 eV energy (ΔG_{solv}) is used to correct the total free energy of OH^* and OOH^*.

In an acidic electrolyte, the ORR can be expressed as:

$$O_2\,(g) + 4H^+ + 4e^- \leftrightarrow 4OH^- \quad (5)$$

The ORR reaction proceeds mainly through the $4e^-$ pathway as the following:

$$O_2\,(g) + H^+ + e^- + * \rightarrow OOH^* \quad (a)$$

$$OOH^* + H^+ + e^- \rightarrow O^* + H_2O \quad (b)$$

$$O^* + H^+ + e^- \rightarrow OH^* \quad (c)$$

$$OH^* + H^+ + e^- \rightarrow H_2O + * \quad (d)$$

where * stands for an active site on the surface, (g) refer to gas phase, respectively. With this approach, the theoretical onset potential (U^{onset}) for ORR at standard conditions is defined as:

$$U^{onset} = |G^{ORR} / e| \quad (6)$$

where G^{ORR} is the potential-determining step defined as the highest free-energy step in the course of ORR, and e is unit charge.

2. Supplementary Figures S1-S23

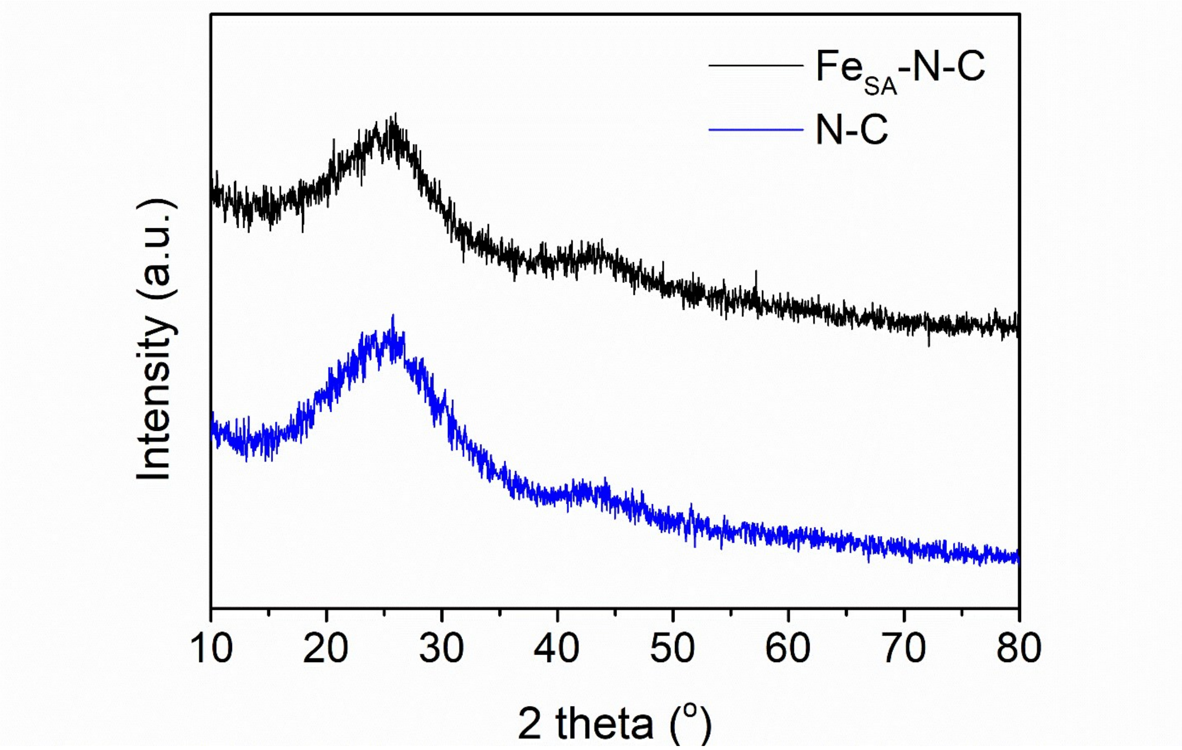

Fig. S1 XRD patterns of the Fe$_{SA}$-N-C and N-C samples.

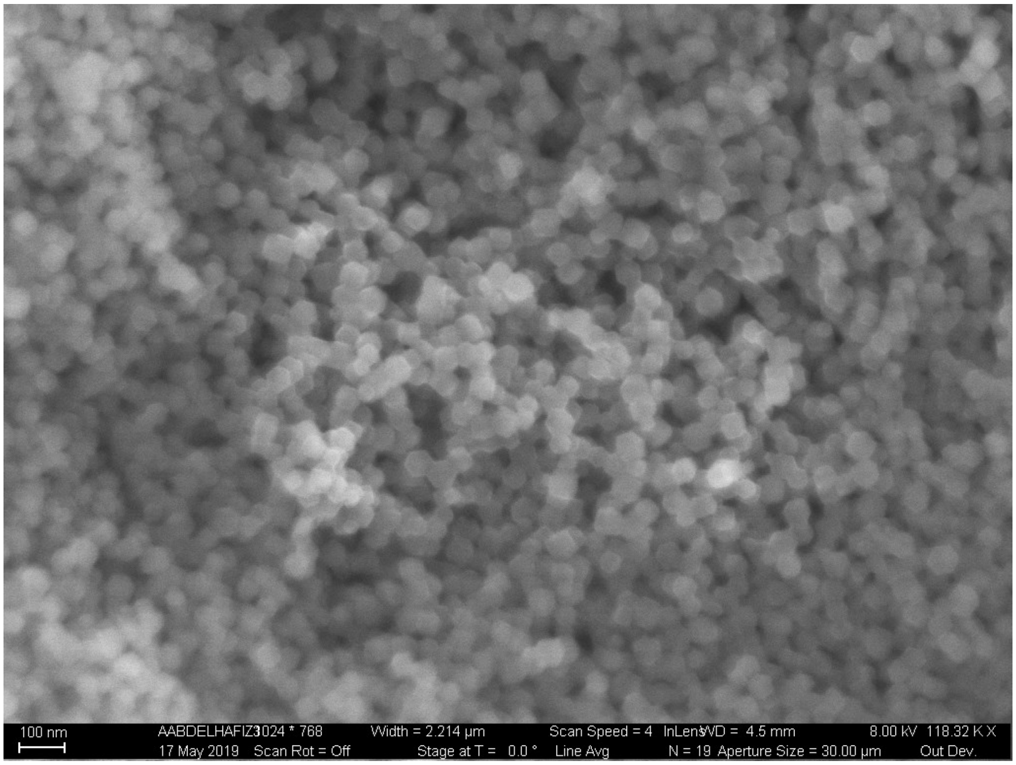

Fig. S2 SEM image of the original ZIF-8 with small particle size.

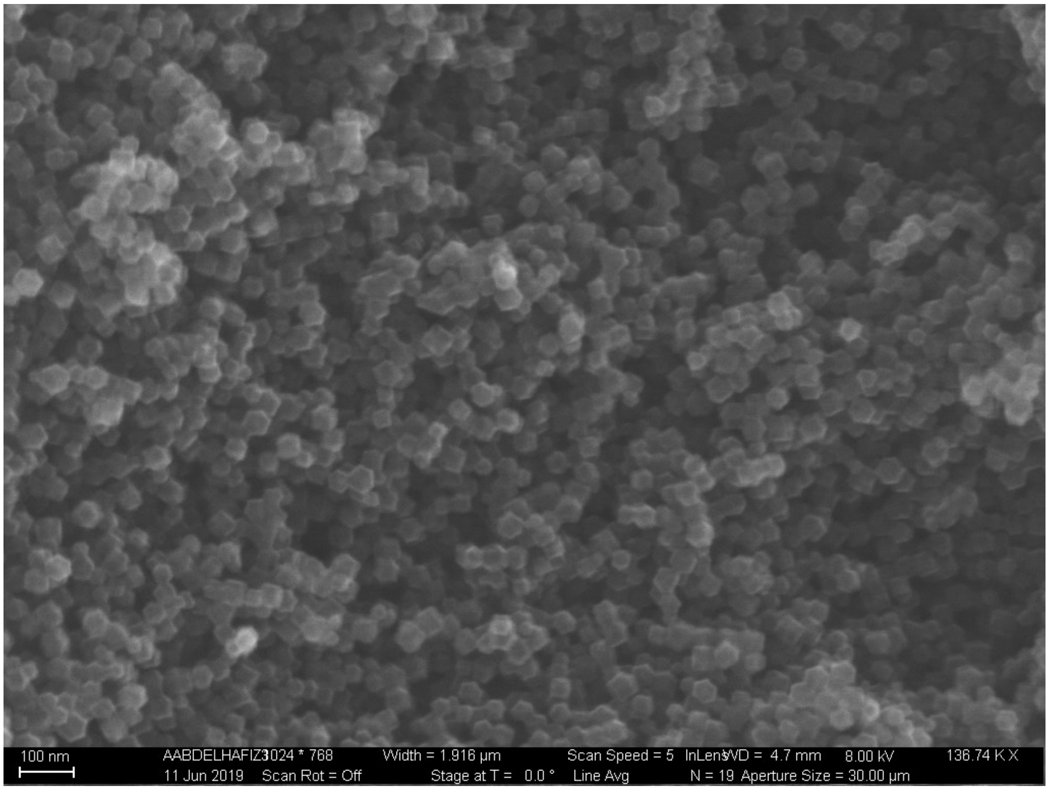

Fig. S3 SEM image of the N-C sample.

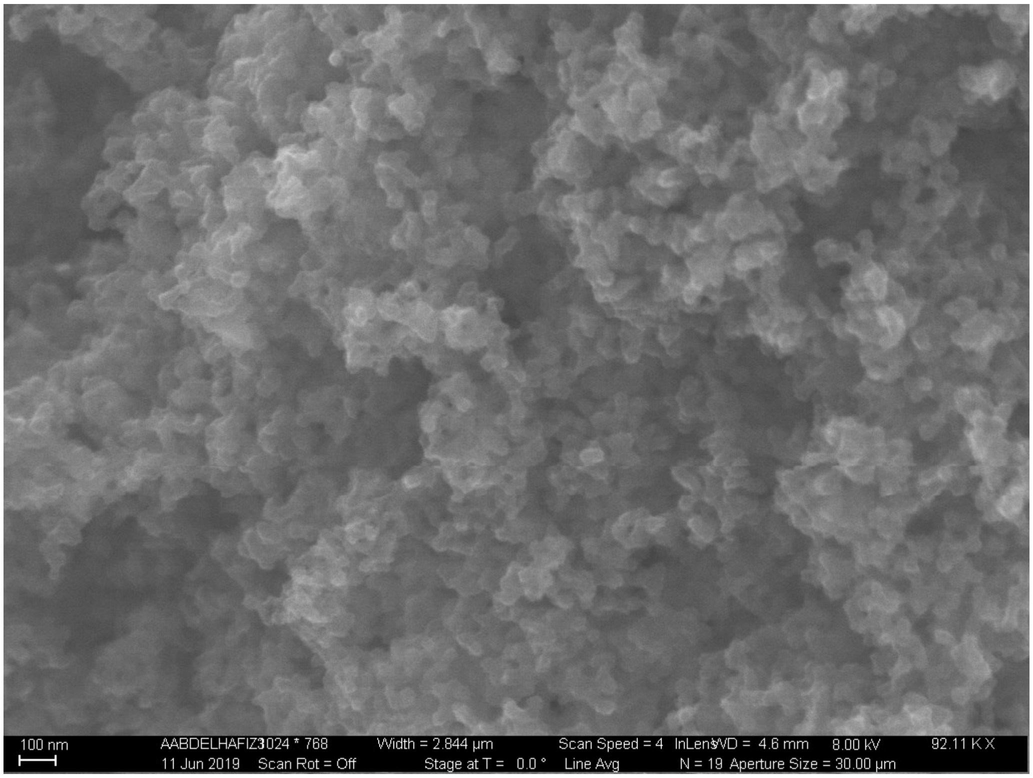

Fig. S4 SEM image of the Fe$_{SA}$-N-C sample.

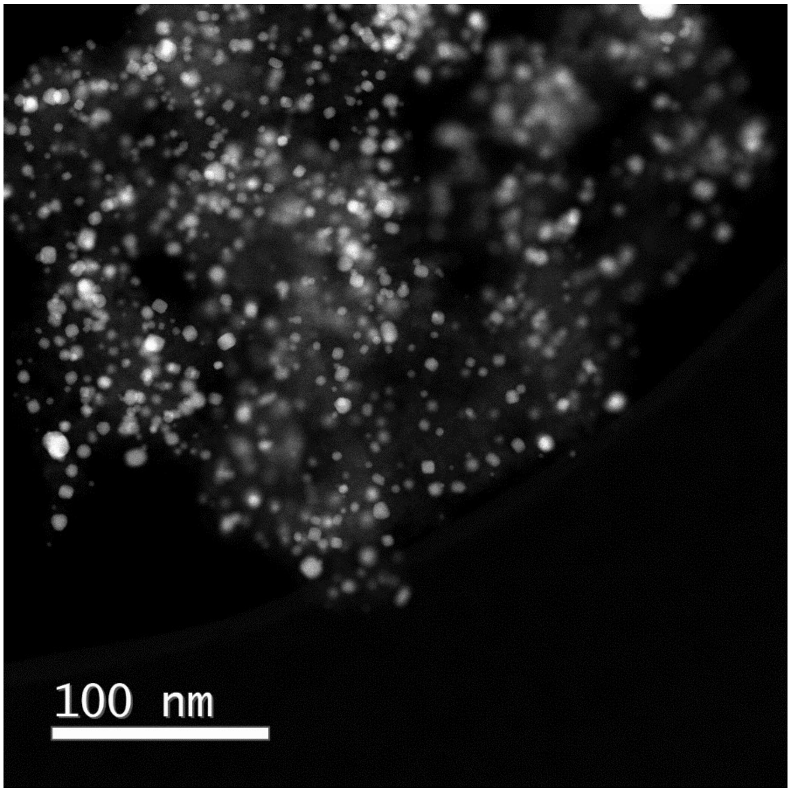

Fig. S5 HAADF-STEM image of the $Pt_A@Fe_{SA}$-N-C sample.

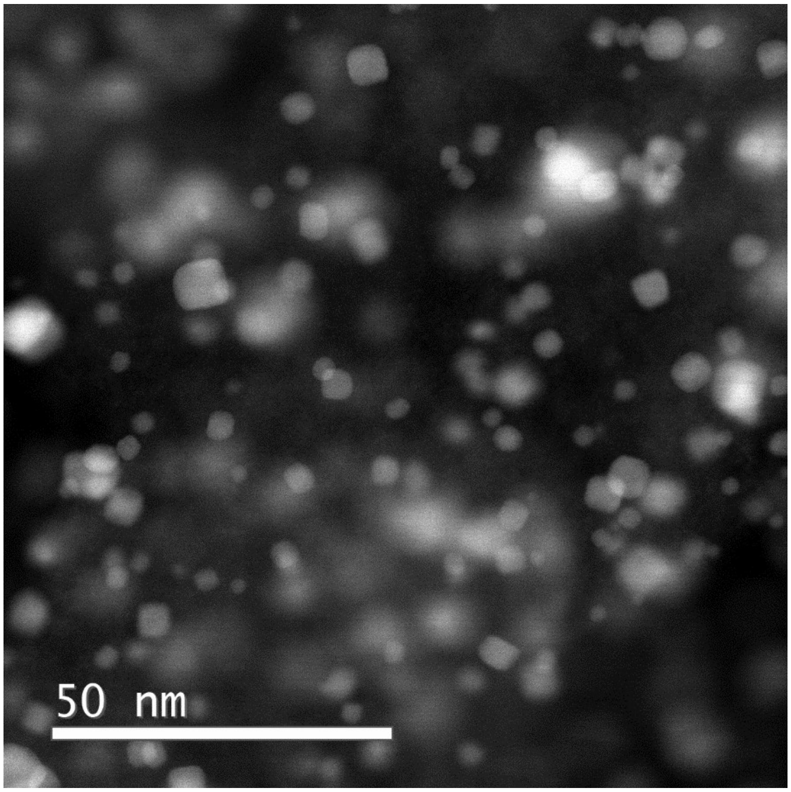

Fig. S6 HAADF-STEM image of the $Pt_A@Fe_{SA}$-N-C sample.

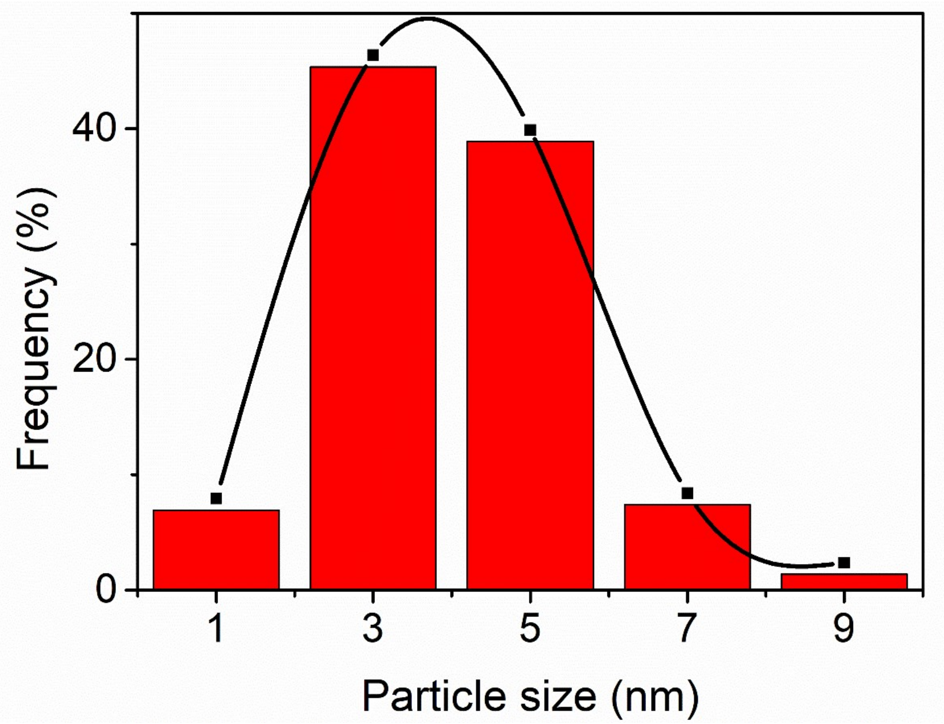

Fig. S7 The particle size distribution histograms of Pt alloy nanoparticles in $Pt_A@Fe_{SA}$-N-C.

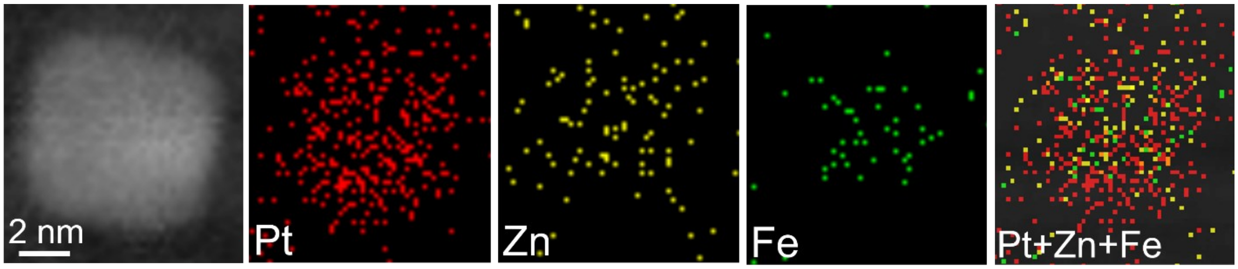

Fig. S8 HAADF-STEM image and corresponding EDX elemental mappings for an individual Pt alloy nanoparticle in $Pt_A@Fe_{SA}$-N-C.

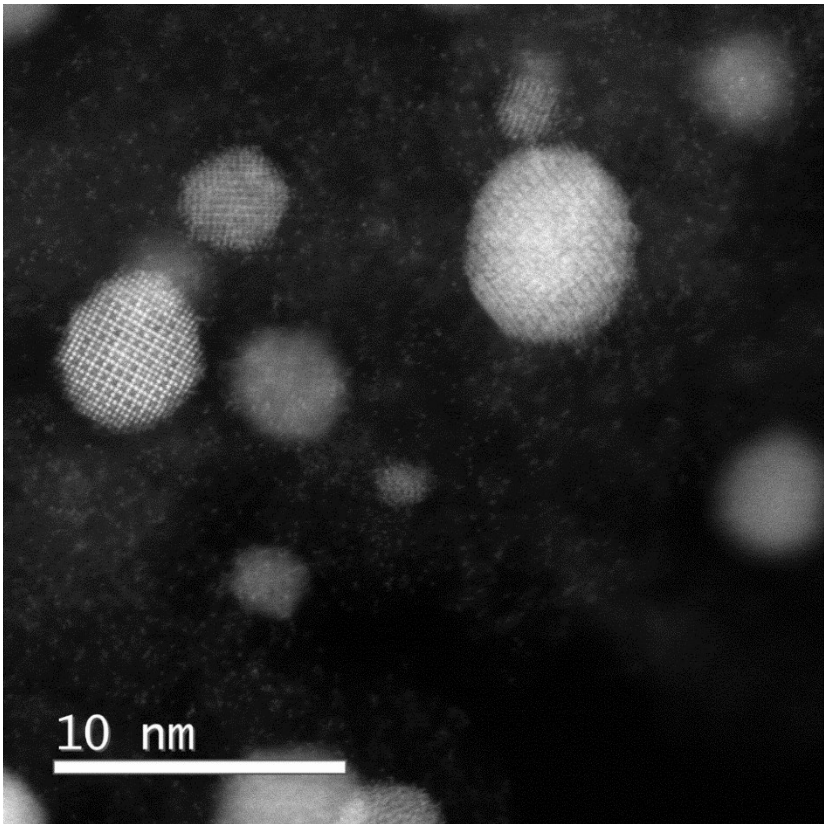

Fig. S9 HAADF-STEM image of the $Pt_A@Fe_{SA}$-N-C sample.

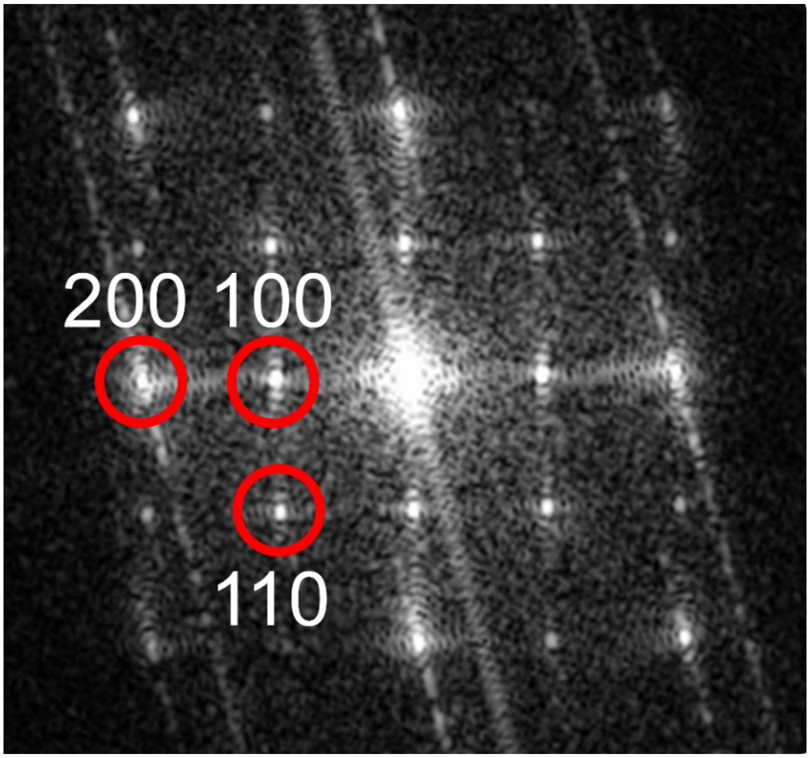

Fig. S10 FFT pattern of the particle in Fig. 1e.

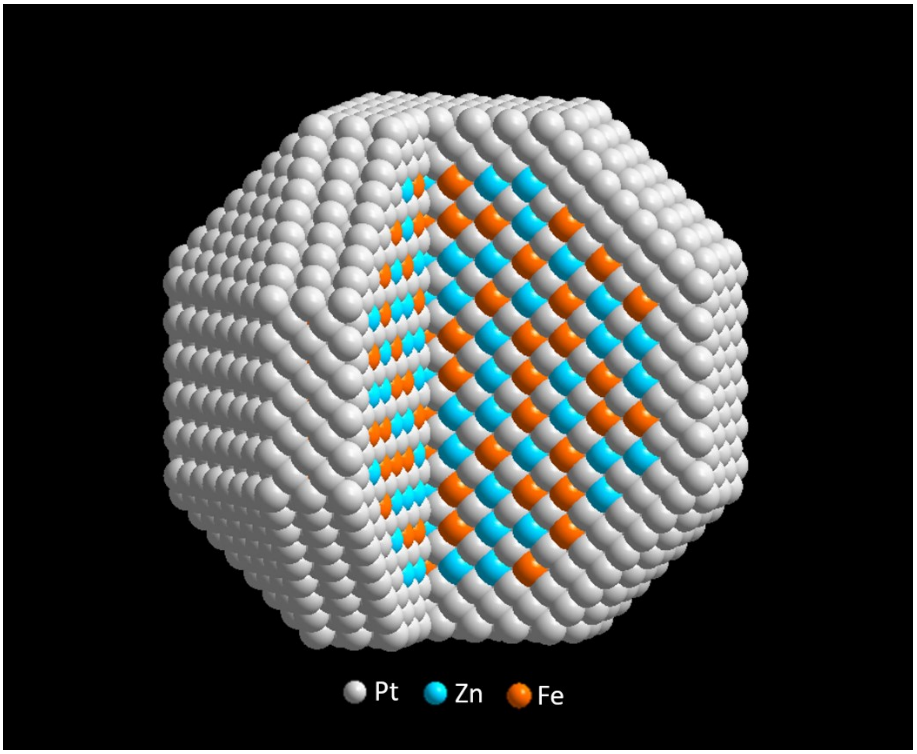

Fig. S11 The idealized atomic structure of the Pt_3M core–shell nanoparticle (the orange, blue and gray spheres present Fe atoms, Zn atoms and Pt atoms, respectively).

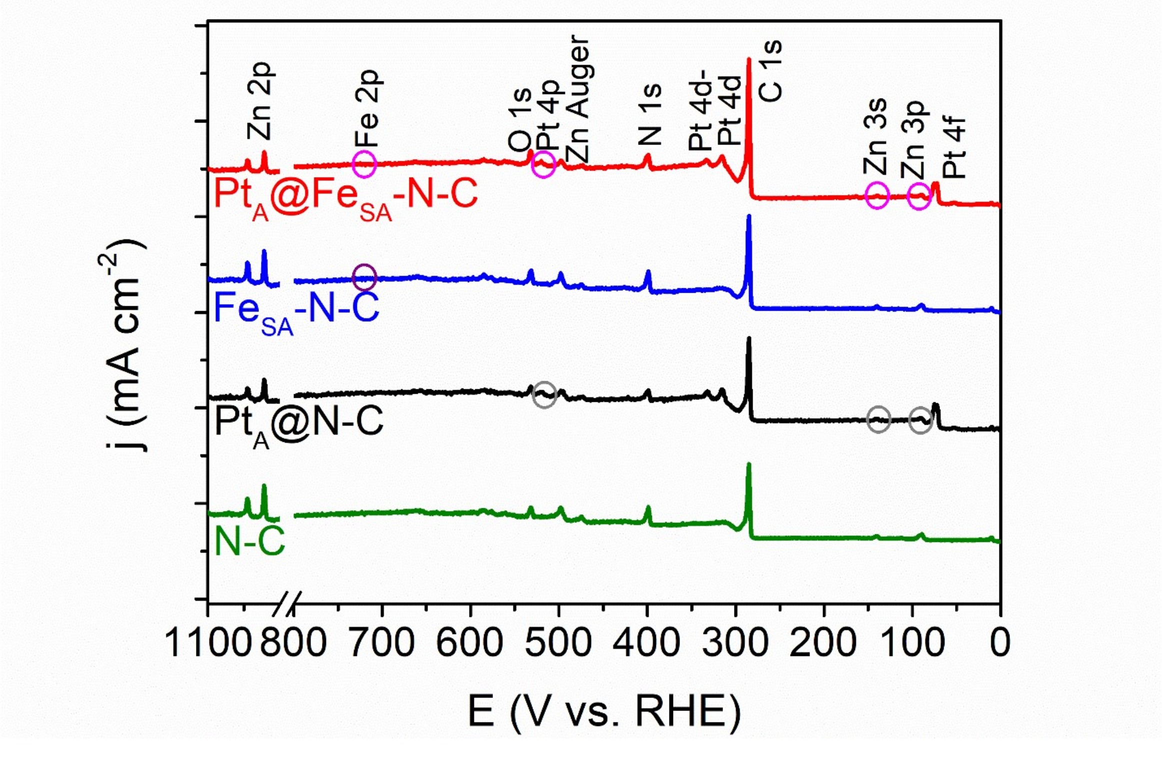

Fig. S12 XPS survey spectra of $Pt_A@Fe_{SA}$-N-C, Fe_{SA}-N-C, $Pt_A@N$-C and N-C.

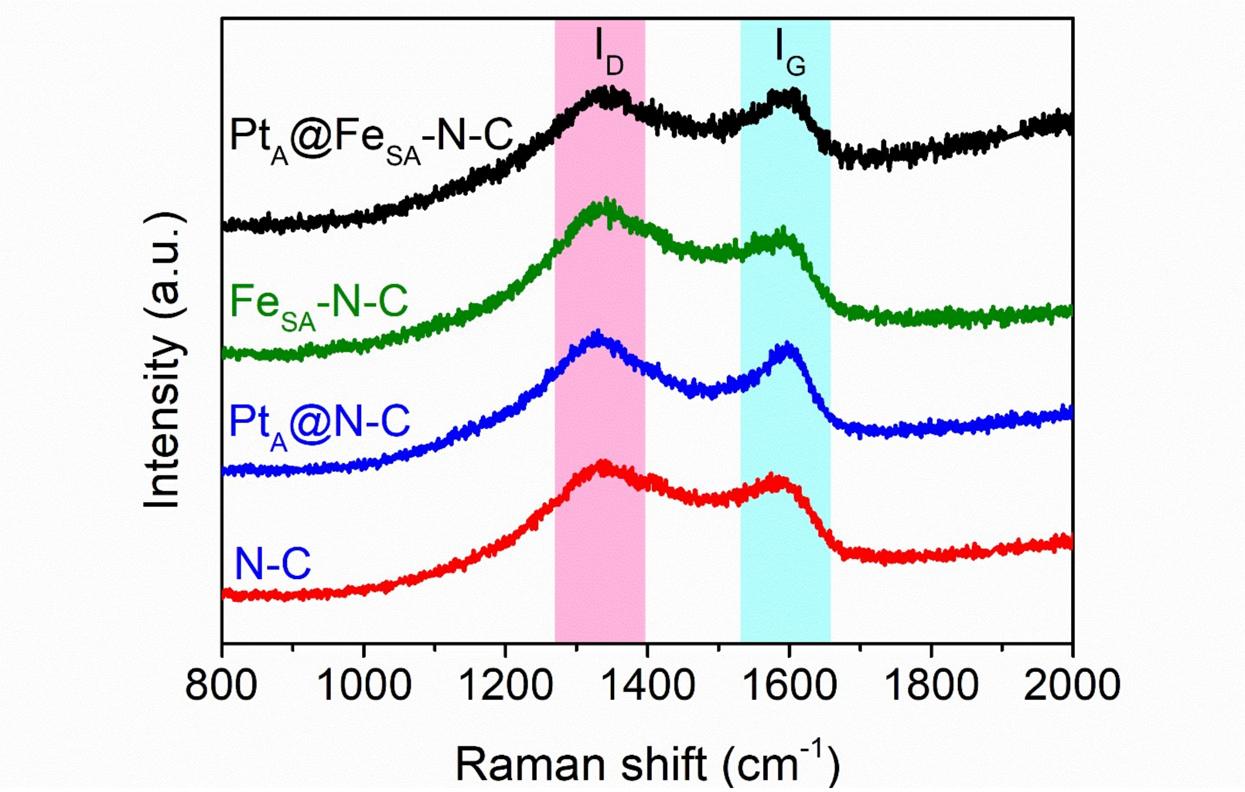

Fig. S13 Raman spectra of $Pt_A@Fe_{SA}$-N-C, Fe_{SA}-N-C, Pt_A@N-C and N-C.

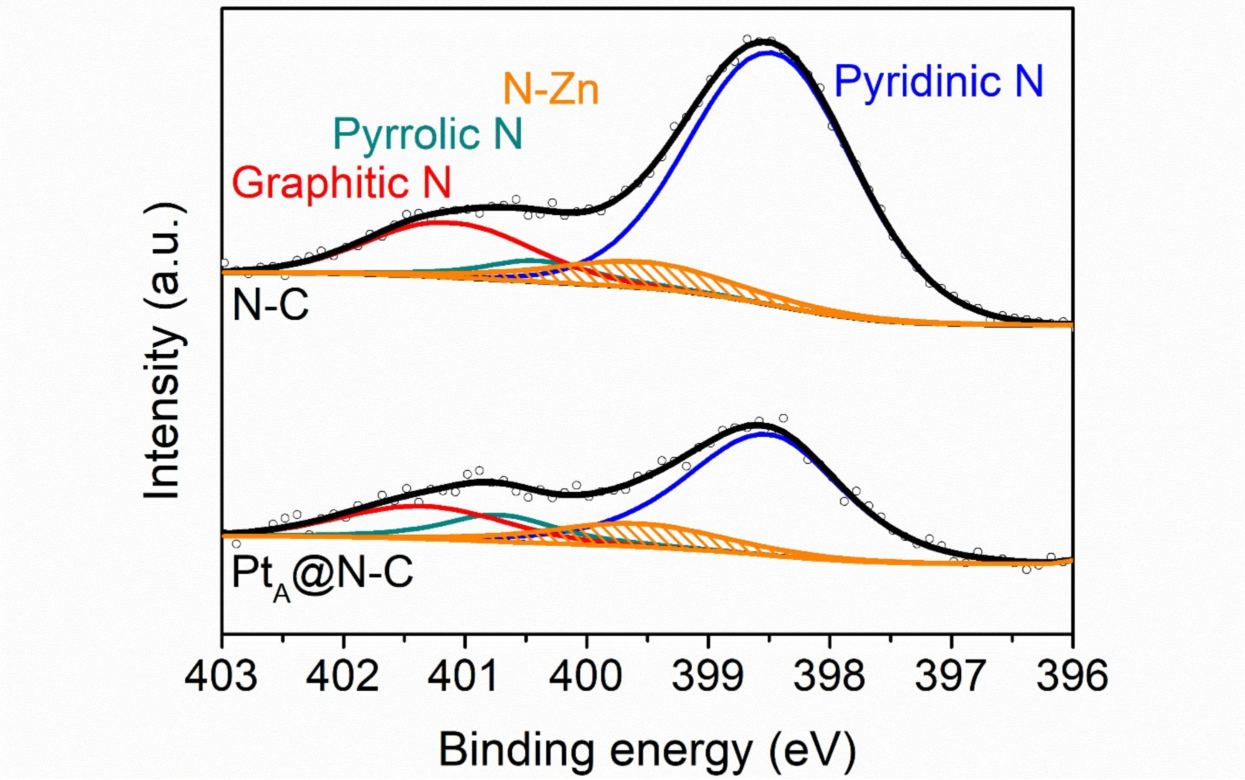

Fig. S14 XPS spectra of N 1s for N-C and Pt_A@N-C.

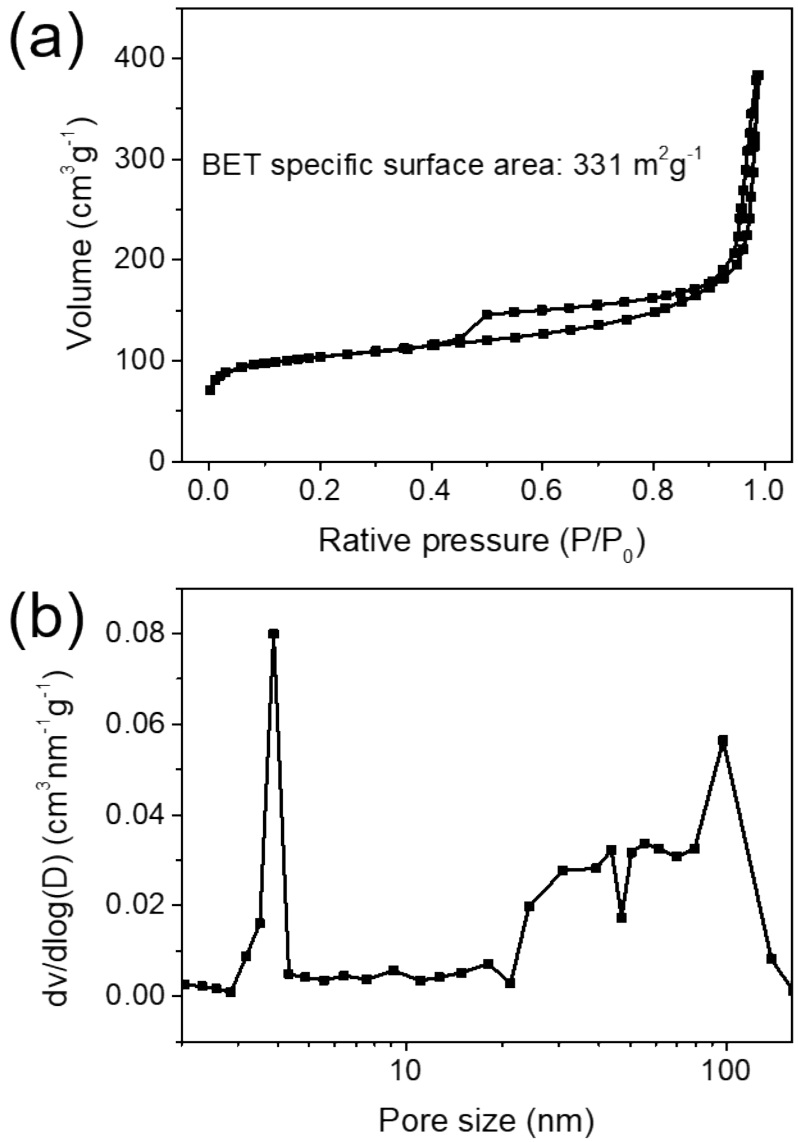

Fig. S15 (a) N_2 adsorption/desorption isotherms, and (b) pore size distribution plot of $Pt_A@Fe_{SA}$-N-C.

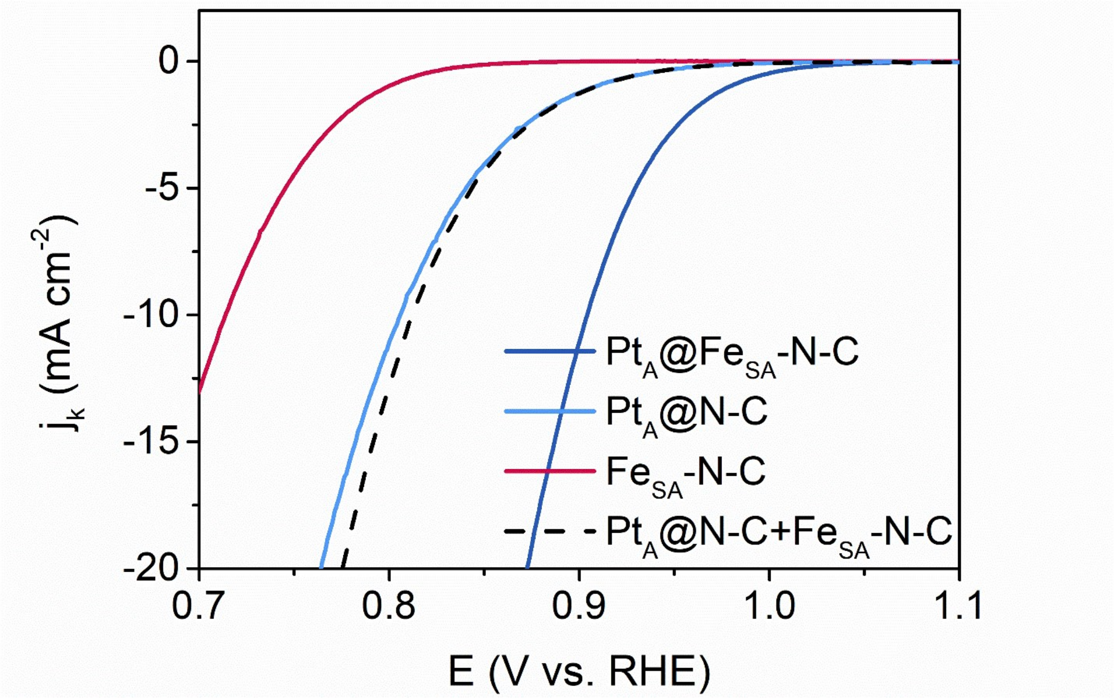

Fig. S16 Kinetic current density of the as-synthesized catalysts calculated from Koutecky-Levich equation.

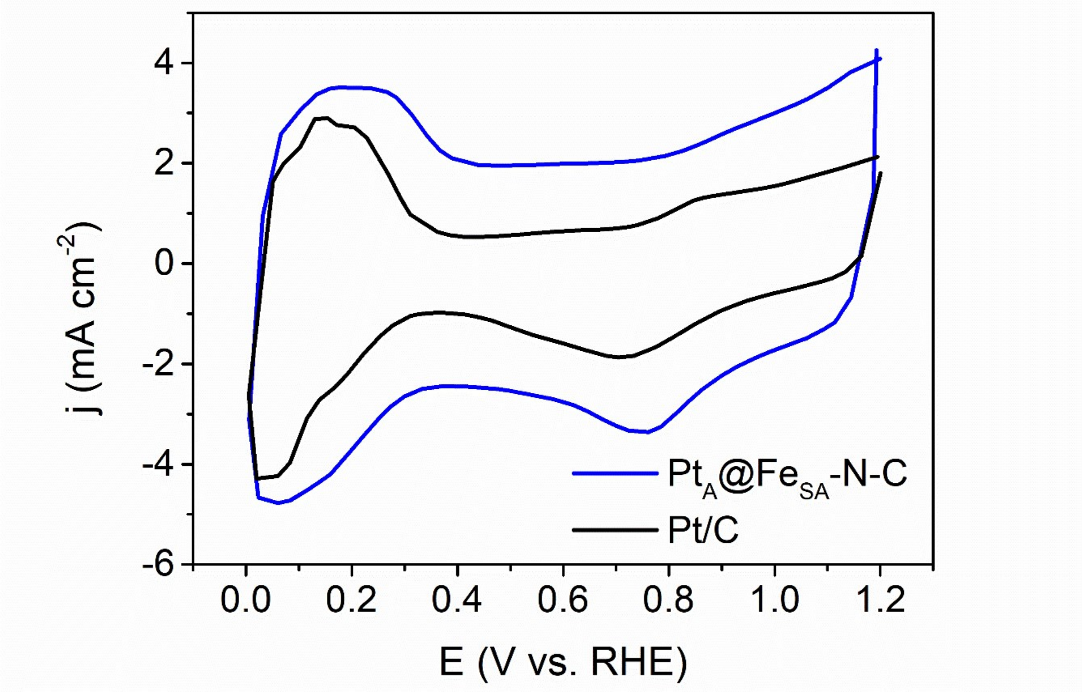

Fig. S17 CV curves of Pt$_A$@Fe$_{SA}$-N-C and Pt/C recorded in N_2-saturated 0.1 M $HClO_4$ aqueous solution at a scan rate of 200 mV s^{-1}.

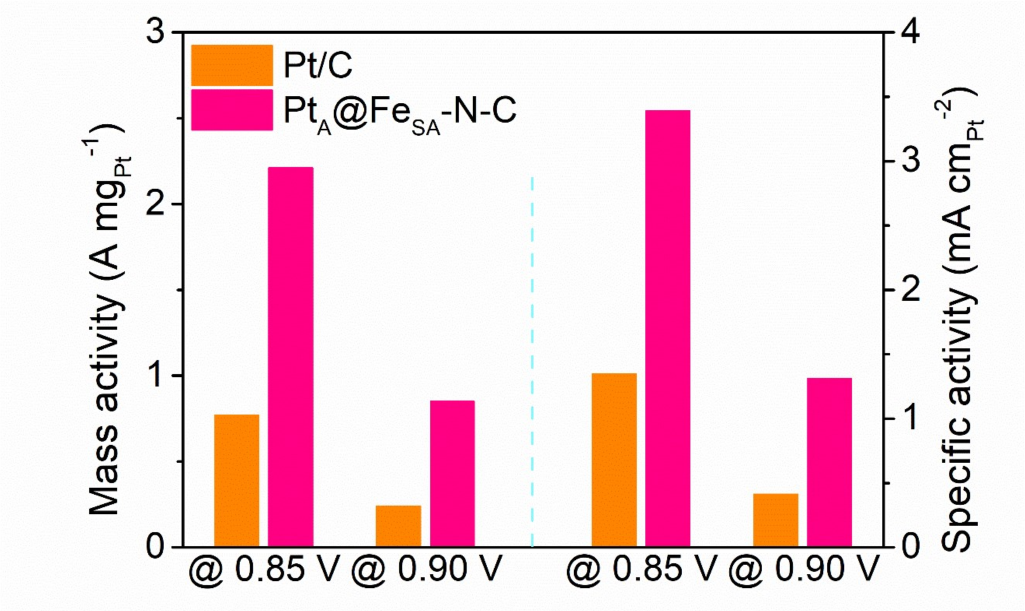

Fig. S18 Comparison of mass activities and specific activities for Pt_A@Fe_{SA}-N-C and Pt/C at 0.85 V and 0.9 V.

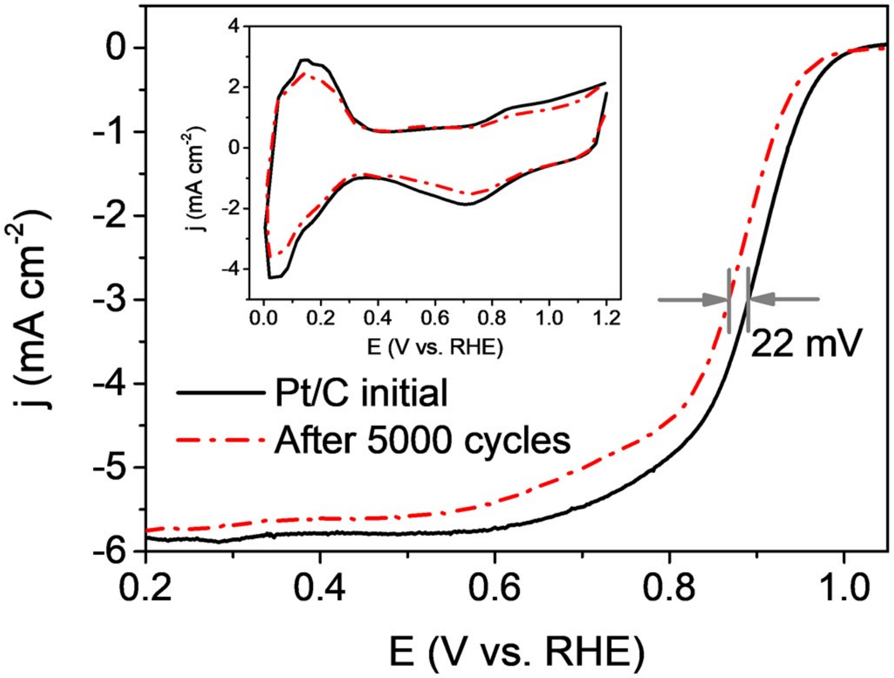

Fig. S19 LSV curves of the commercial Pt/C recorded at a scan rate 10 mV s^{-1} and a rotation rate of 1600 rpm in O_2-saturated 0.1 M $HClO_4$ before and after the durability test; the durability was examined with an ADT by cycling in the potential range of 0.6-1.0 V at a scan rate of 50 mV s^{-1}. The inset shows the CV curves at a scan rate of 200 mV s^{-1} before and after ADT.

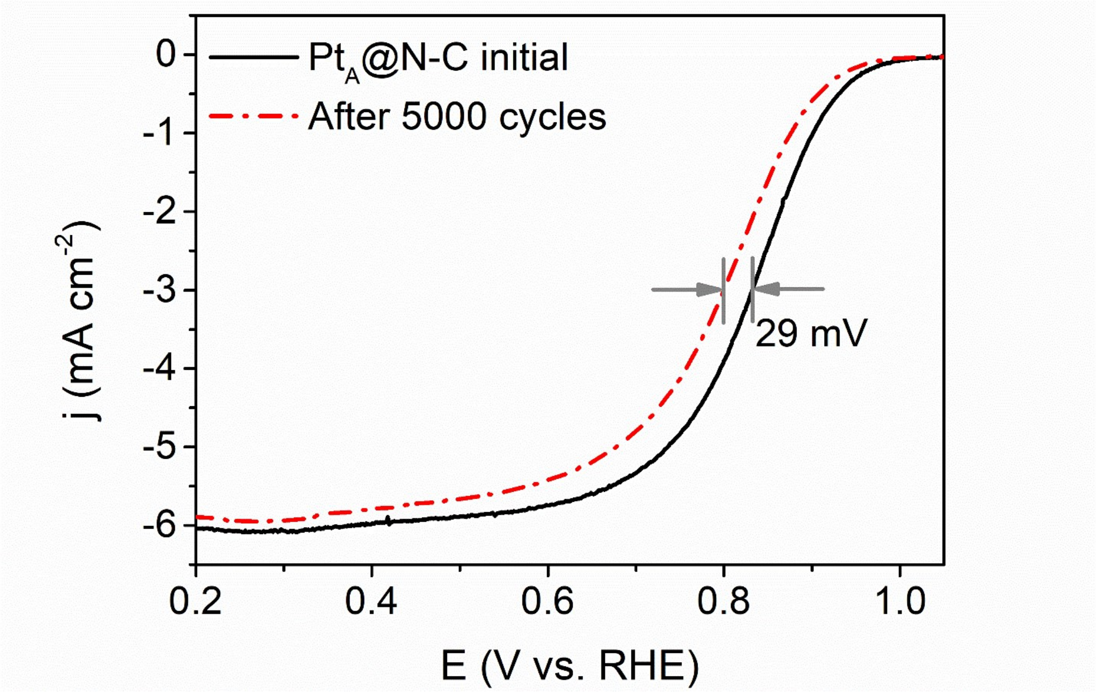

Fig. S20 LSV curves of a Pt$_A$@N-C sample recorded at a scan rate 10 mV s^{-1} and a rotation rate of 1600 rpm in O$_2$-saturated 0.1 M HClO$_4$ before and after durability test; the durability was examined with an ADT by cycling in the potential range of 0.6-1.0 V at a scan rate of 50 mV s^{-1}.

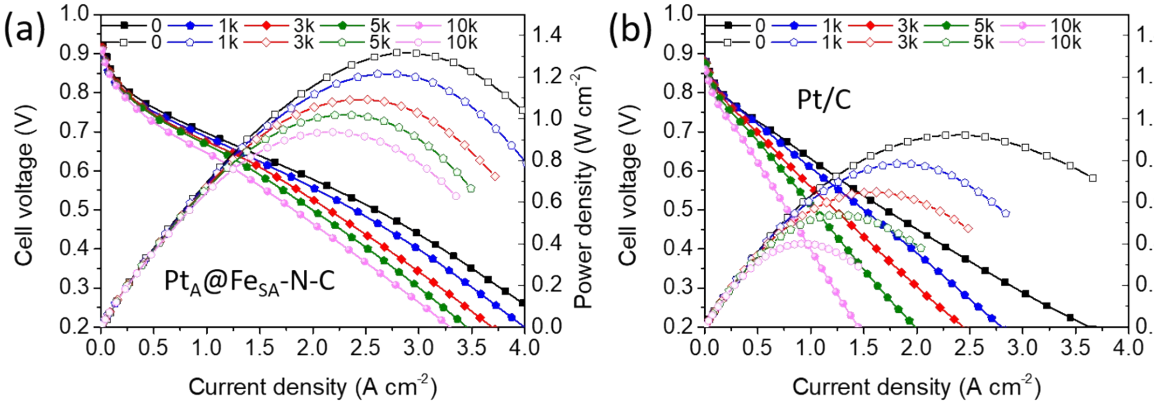

Fig. S21 *I-V* (solid symbols and lines) and *I-P* (hollow symbols and dashed lines) curves measured after CV cycles for fuel cells with (a) Pt$_A$@Fe$_{SA}$-N-C and (b) Pt/C as the cathode catalysts.

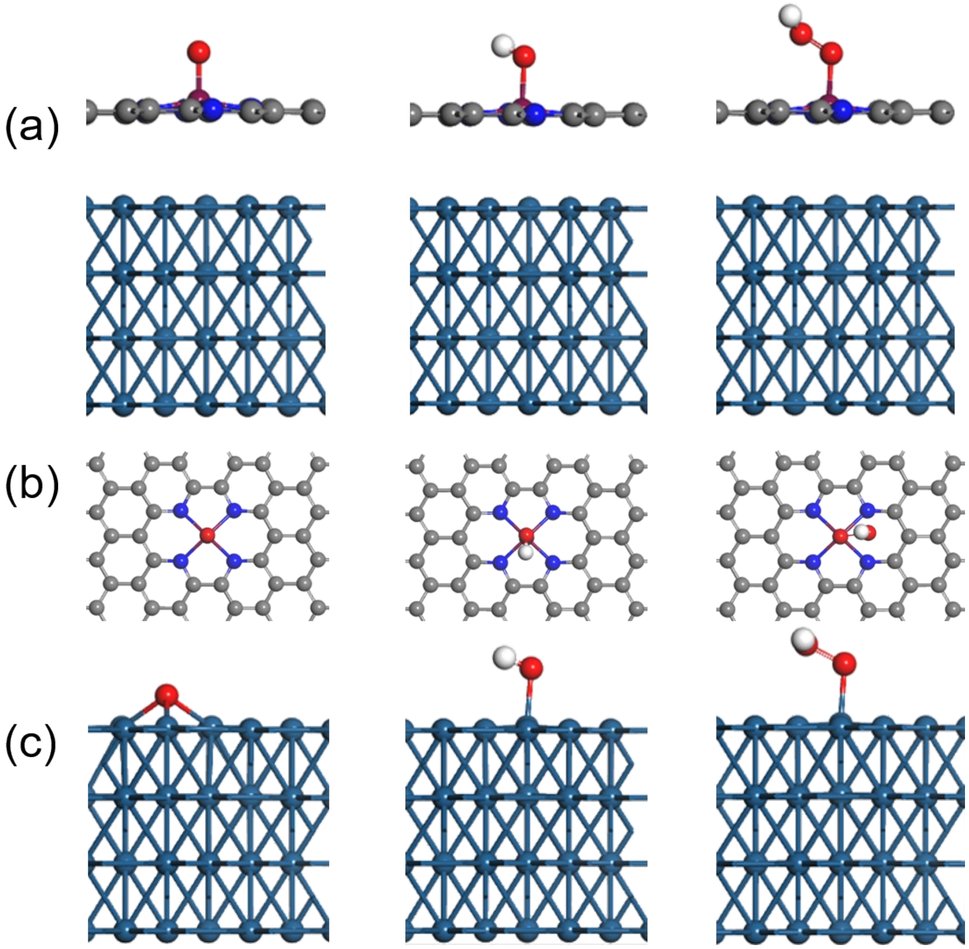

Fig. S22 Configurations of adsorbates on (a) Pt (100)/Fe-N_4, (b) Fe-N_4 and (c) Pt (100).

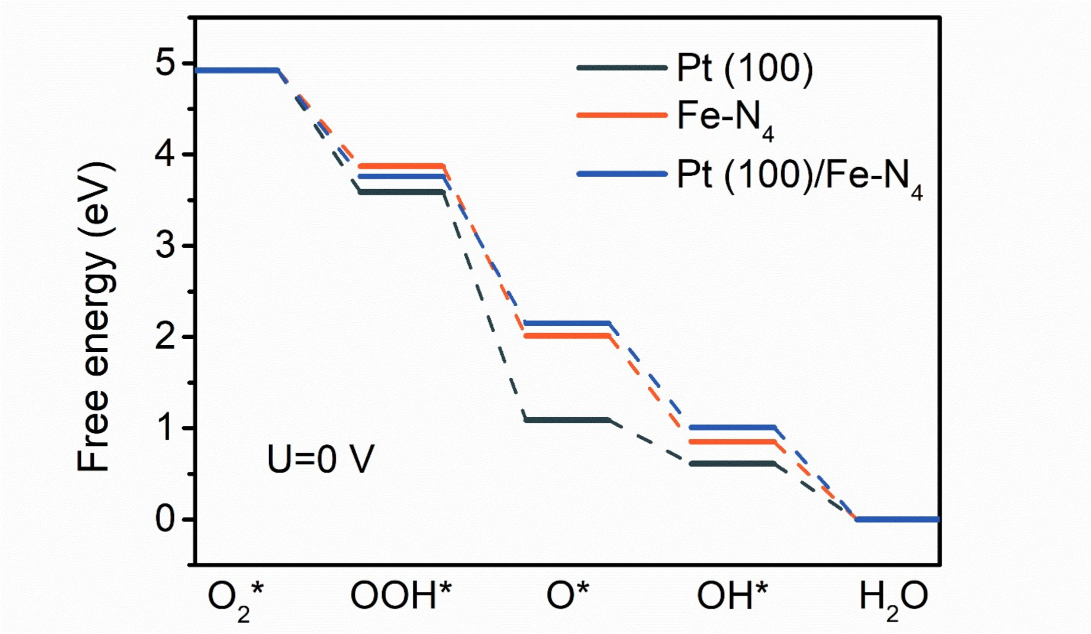

Fig. S23 Free-energy path of the ORR at U=0 V for the three models constructed.

3. Supplementary Table S1-S6

Table S1. Elemental quantification determined by XPS for different samples.

Percentage	C (at%)	N (at%)	O (at%)	Zn (at%)	Fe (at%)	Pt (at%)
Fe_{SA}-N-C	75.43	12.99	6.50	4.13	0.95	--
Pt_A@Fe_{SA}-N-C	83.90	7.43	4.64	1.93	0.93	1.17
N-C	76.48	13.36	5.11	5.05	--	--
Pt_A@N-C	82.23	8.43	4.87	2.44	--	2.03

Table S2. Structural parameters extracted from the EXAFS fitting of Fe_{SA}-N-C. (S_0^2=1)

Sample	Scattering pair	CN	R(Å)	$\sigma^2(10^{-3}Å^2)$	ΔE_0(eV)	R factor
Fe_{SA}-N-C	Fe-N	4.175	1.977	7.68	-3.03	0.018

S_0^2 is the amplitude reduction factor; CN is the coordination number; R is the interatomic distance (the bond length between central atoms and surrounding coordination atoms), σ^2 is Debye-Waller factor (a measure of thermal and static disorder in absorber-scatterer distances); ΔE_0 is edge-energy shift (the difference between the zero kinetic energy value of the sample and that of the theoretical model). R factor is used to value the goodness of the fitting.

Table S3. Comparison of the ORR activity of Pt_A@Fe_{SA}-N-C with various recently reported Pt-based catalysts.

Catalysts	electrolyte	Pt loading (ug_{Pt} cm^{-2})	Half-wave potential (V vs. RHE)	References
Pt_A@Fe_{SA}-N-C	**0.1 M $HClO_4$**	**13**	**0.923**	**This work**
NPG–Pd–Pt	0.1 M $HClO_4$	20	0.892	*Nat. Energy* **2017**, 2, 1-9
Pt/NG-TiON	0.5 M H_2SO_4	360	0.868	*Appl. Catal., B* **2019**, 118414
Pt/TiO2-C	0.1 M $HClO_4$	20.4	0.876	*Appl. Catal., B* **2018**, 237, 228-236
PtBi/C	0.1 M $HClO_4$	10	0.886	*ACS Catal.* **2018**, 8, 5581−5590
Pt/40Co-NC-900	0.1 M $HClO_4$	60	0.92	*Nano Lett.* **2018**, 18, 4163−4171
PtNi-BNCs/C	0.1 M $HClO_4$	6.8	0.923	*Science* **2019**, 366, 850–856
Pt/CNTs	0.1 M $HClO_4$	20	0.85	*Chem. Mater.* **2017**, 29, 9579−9587
$PtCo_3$-H600	0.1 M $HClO_4$	12	0.905	*Adv. Funct. Mater.* **2019**, 29 1902987
Co_2P/Pt	0.1 M $HClO_4$	10.2	0.912	*Nano Lett.* **2018**, 18, 7870−7875
D-O_2-Pt NWs	0.1 M $HClO_4$	5.1	0.882	*J. Mater. Chem. A* **2019**, 7, 24830-24836
Pt-Pd SBCNC	0.1 M $HClO_4$	11.4	0.912	*Appl. Catal., B* **2019**, 251, 49-56

Table S4. Adsorption free energies (eV) of the reaction intermediate O* (ΔG_O), OH* (ΔG_{OH}), and OOH* (ΔG_{OOH}), on the Pt (100), Fe-N_4 and Pt (100)/Fe-N_4 electrocatalyst systems.

	ΔG_O	ΔG_{OH}	ΔG_{OOH}
Pt (100)	1.09	0.61	3.59
Fe-N_4	2.01	0.85	3.87
Pt (100)/Fe-N_4	2.15	1.01	3.76

Table S5. Reaction free energies (eV vs RHE) of elementary step for ORR at U= 0 V, and the computed overpotential for ORR (U^{onset}) based on the Pt (100), Fe-N_4 and Pt (100)/Fe-N_4 electrocatalyst systems.

	ΔG_1	ΔG_2	ΔG_3	ΔG_4	U^{onset}
Pt (100)	-1.33	-2.50	-0.48	-0.61	0.48
Fe-N_4	-1.05	-1.86	-1.16	-0.85	0.85
Pt (100)/Fe-N_4	-1.15	-1.61	-1.14	-1.01	1.01

Table S6. Reaction free energies (eV vs RHE) of elementary step for ORR at U= 0.9 V, and the computed overpotential for ORR (U^{onset}) based on the Pt (100), Fe-N_4 and Pt (100)/Fe-N_4 electrocatalyst systems.

	ΔG_1	ΔG_2	ΔG_3	ΔG_4	U^{onset}
Pt (100)	-0.43	-1.60	0.42	0.29	0.48
Fe-N_4	-0.15	-0.96	-0.26	-0.05	0.85
Pt (100)/Fe-N_4	-0.25	-0.71	-0.24	-0.11	1.01

4. Reference

1. J. Quinson, M. Inaba, S. Neumann, A. A. Swane, J. Bucher, S. B. Simonsen, L. Theil Kuhn, J. J. Kirkensgaard, K. M. Jensen and M. Oezaslan, *ACS Catal.*, 2018, **8**, 6627-6635.
2. Y. Garsany, I. L. Singer and K. E. Swider-Lyons, *J. Electroanal. Chem.*, 2011, **662**, 396-406.
3. B. Zhao, J. Song, R. Ran and Z. Shao, *Int. J. Hydrogen Energy*, 2012, **37**, 1133-1139.
4. B. Zhao, L. Sun, R. Ran and Z. Shao, *Solid State Ionics*, 2014, **262**, 313-318.
5. G. Kresse and J. Hafner, *Phys. Rev. B*, 1993, **47**, 558.
6. G. Kresse and J. Furthmüller, *Phys. Rev. B*, 1996, **54**, 11169.
7. G. Kresse and J. Furthmüller, *Comp. Mater. Sci.*, 1996, **6**, 15-50.
8. J. P. Perdew, K. Burke and M. Ernzerhof, *Phys. Rev. Lett.*, 1996, **77**, 3865.
9. J. P. Perdew and Y. Wang, *Phys. Rev. B*, 1992, **45**, 13244.
10. P. E. Blöchl, *Phys. Rev. B*, 1994, **50**, 17953.
11. S. Grimme, J. Antony, S. Ehrlich and H. Krieg, *J. Chem. Phys.*, 2010, **132**, 154104.
12. S. Dudarev, G. Botton, S. Savrasov, C. Humphreys and A. Sutton, *Phys. Rev. B*, 1998, **57**, 1505.
13. J. Jiang, F. Sun, S. Zhou, W. Hu, H. Zhang, J. Dong, Z. Jiang, J. Zhao, J. Li and W. Yan, *Nat. Commun.*, 2018, **9**, 2885.
14. H. Xu, D. Cheng, D. Cao and X. C. Zeng, *Nat. Catal*, 2018, **1**, 339-348.
15. J. K. Nørskov, J. Rossmeisl, A. Logadottir, L. Lindqvist, J. R. Kitchin, T. Bligaard and H. Jónsson, *J. Phys. Chem. B*, 2004, **108**, 17886-17892.
16. J. H. Montoya, M. Garcia-Mota, J. K. Nørskov and A. Vojvodic, *Phys. Chem. Chem. Phys.*, 2015, **17**, 2634-2640.
17. F. Calle-Vallejo, J. Martínez, J. García-Lastra, E. Abad and M. Koper, *Surf. Sci.*, 2013, **607**, 47-53.
18. K. Mao, W. Zhang, J. Dai and X. C. Zeng, *Nanoscale*, 2019, **11**, 19422-19428.
19. P. Li, W. Zhang, C. Liang and X. C. Zeng, *Nanoscale*, 2019, **11**, 19806-19813.